Investigation of Thermal Behaviors of Poly(3-Chloro-2-Hydroxypropyl Methacrylate) modified with Amine-Rich Groups

Amin Gruplarla Modifiye Edilmiş Poli (3-Kloro-2-Hidroksipropil Metakrilat) Termal Davranışlarının İncelenmesi

Research Article

Duygu Alparslan
Department of Chemical Engineering, Van Yüzüncü Yıl University, Campus, Van, Turkey.

ABSTRACT

Poly(3-chloro-2-hydroxypropyl methacrylate) (p(HPMA-Cl)) microgels were synthesized through surfactant-free emulsion polymerization technique (SFEP) by addition of ethylene glycol dimethacrylate (EGDMA) as a cross-linker. Next, the obtained p(HPMA-Cl) microgels were modified by using tris(2-aminoethyl)amine (TAEA) and poly(ethyleneimine) (PEI) as modifying agents. After modification, the synthesized microgels were named as poly(3-chloro-2-hydroxypropyl methacrylate)-tris(2-aminoethyl)amine (p(HPMA)-TAEA) and poly(3-chloro-2hydroxypropyl methacrylate)-poly(ethyleneimine) (p(HPMA)-PEI) microgels. Thermal decomposition kinetics of these microgels which were based on the p(HPMA-Cl) were then evaluated using thermo-gravimetric analysis. The kinetic parameters for the degradation reactions of p(HPMA-Cl)-based microgels, including the correlation coefficients and activation energy and mechanisms, were determined using the TGA-DTA data. Experimental data for p(HPMA-Cl), p(HPMA)-TAEA and p(HPMA)-PEI microgels were computed through twenty-four different thermal degradation models to evaluate the best-fitted model. The activation energies (Ea) of p(HPMA-Cl), p(HPMA)-TAEA and (p(HPMA)-PEI) microgels composites were determined by the Kissinger-Akahira Sunose (KAS), Flynn-Wall-Ozawa (FWO), Coats-Redfern, Ozawa and Friedman methods. Based on the results, nucleation-nuclei growth models seem to be the most suitable for these microgels.

Key Words
p(HPMA-Cl) microgels, modified p(HPMA-Cl), thermal behavior of p(HPMA-Cl) microgels, thermal degradation, activation energy.

ÖZ

Poli (3-kloro-2-hidroksipropil metakrilat) (p(HPMA-Cl)) mikrojelleri, surfektan içermeyen emülsiyon polimerizasyon tekniği (SFEP) ile sentezlenmiştir. Daha sonra p(HPMA-Cl) mikrojel, modifiye edici maddeler olarak tris(2-aminoetil) amin (TAEA) ve poli(etilenimin) (PEI) kullanılarak modifiye edilmiştir. Modifiye mikrojeller poli(3-kloro-2-hidroksipropil metakrilat)-tris(2-aminoetil) amin (p(HPMA)-TAEA) ve poli (3-kloro-2-hidroksipropil metakrilat)-poli (etilenimin) p(HPMA)-PEI) olarak adlandırılmış. p(HPMA-Cl) temelli mikrojellerin termal bozunma kinetikleri, termogravimetrik analiz kullanılarak değerlendirilmiştir. Korelasyon katsayıları, aktivasyon enerjisi ve mekanizmaları dahil olmak üzere p(HPMA-Cl) temelli mikrojellerin bozunma reaksiyonları için kinetik parametreler, TGA-DTA verilerinden belirlenmiştir. p(HPMA-Cl), p(HPMA)-TAEA ve p(HPMA)-PEI mikrojelleri için en uygun modeli bulmak için deneysel veriler yirmi dört farklı termal bozunma modeli kullanılarak hesaplanmıştır. p(HPMA-Cl), p(HPMA)-TAEA ve p(HPMA)-PEI) mikrojel kompozitlerinin aktivasyon enerjileri (Ea) Kissinger-Akahira Sunose (KAS), Flynn-Wall-Ozawa (FWO) Coats-Redfern, Ozawa ve Friedman, yöntemleri ile hesaplanmıştır.

Anahtar Kelimeler
p(HPMA-Cl) mikrojel, modifye p(HPMA-Cl), p(HPMA-Cl) mikrojelinin termal davranışı, termal bozunma, aktivasyon enerjisi

Article History: Received: Jun 12, 2018; Revised: Oct 02, 2018; Accepted: Nov 12, 2018; Available Online: Nov 22, 2018.

DOI: 10.15671/HJBC.2018.267

Correspondence to: D. Alpaslan, Department of Chemical Engineering, Van Yüzüncü Yıl University, Campus, Van, Turkey.
Tel: +90 432 218 0018 Fax: +90 432 218 0018 E-Mail: alpaslanduygu@gmail.com

INTRODUCTION

Solid-state phase chemistry attracted a great deal attention in the fields of chemistry, pharmacology, environmental and mining sciences in recent years [1-13]. Solid-state kinetic reactions have always drawn great attention and are seen as challenging issues in chemical researches [1-6,14,15]. These reactions can mechanistically be classified according to the diffusion [7,8,16], geometrical contraction [8,16], nucleation and reaction order models [1-3,10,11,17]. Empirically, on the other hand, these reactions are verified either isothermally or non-isothermally. The isothermal method is based on the degradation of samples at different temperatures [18-20]. According to this method, the data for the α-time point is produced at each temperature segment. In the non-isothermal method, degradation is investigated under constant temperature increase. The non-isothermal method is commonly used due to its high sensitivity compared to the isothermal method. A lot of kinetics-related data can be obtained from the thermogravimetric data, like the activation energy and exponential factor. In the course of the kinetic analysis, the kinetic parameters could be determined by some mathematical approaches, like the Kissinger-Akahira Sunose (KAS) [15], Flynn-Wall-Ozawa (FWO) [12], Coats-Redfern [6,12], Ozawa [11,19] and Friedman [11] methods. Coats-Redfern kinetic method uses the integral form of the non-isothermal rate law. Flynn-Wall-Ozawa (FWO) method is derived from the integral method. Flynn-Wall-Ozawa (FWO) method is an integral isothermal method similar to the Kissinger-Akahira Sunose (KAS) method [18-20]. To obtain thermogravimetric data, thermogravimetric analysis (TGA) is the most widely used and the sensitive method in the literature. TGA is mainly used to investigate the thermal decomposition of polymeric materials depending on the change in the mass of a sample as a function of time or temperature in a controlled atmosphere [3,12-15,17]. These changes can be either mass loss or gain due to decomposition, dehydration, oxidation or loss of volatiles [21-23].

The aim of this study is to determine the thermal behaviors of the prepared p(HPMA-Cl), p(HPMA)-TAEA and p(HPMA)-PEI microgels for the potential of high-temperature applications of the compounds, like in catalytic reactions or solar cell applications. Firstly, p(HPMA-Cl) microgel was synthesized by the SFEP technique and then modified either with TAEA or PEI. The kinetics of the thermal degradation of p(HPMA-Cl) microgels modified using different agents (TAEA or PEI) were then investigated by TGA under an argon atmosphere with heating rates of 2, 6, and 10 °C/min. Finally, their activation energy values were calculated by Kissinger-Akahira Sunose (KAS), Flynn-Wall-Ozawa (FWO), Coats-Redfern, Ozawa and Friedman methods.

MATERIALS and METHODS

Materials

(a)3-chloro-2-hydroxypropyl methacrylate (HPMA-Cl), (b)ethylene glycol dimethacrylate (EGDMA, 98%), (c)2,2′-azobis(2-methylpropionamidine) dihydrochloride (AAPH), (d)tris(2-aminoethyl) amine (TAEA, 96%), and (e)poly(ethyleneimine) solutions (PEI, average Mn ~1,200, average and Mw ~1300 by LS, 50 wt. % in H_2O) were purchased from Aldrich. Ethanol (EtOH, 98%) was purchased from Kimetsan, while N,N-dimethylformamide (DMF, 99%) was purchased from Merck. Distilled water (DI, 18.2 MΩ cm; Millipore Direct-Q3UV) was also used throughout this study.

The Synthesis of p(HPMA-Cl) Microgels

P(HPMA-Cl) microgels were synthesized by the surfactant-free emulsion polymerization (SFEP) technique [24]. Briefly, 145 mL DI water was poured into a one-necked flask and 10.05 mmol HPMA-Cl and 0.25 mmol EGDMA were added and mixed at 600 rpm for 10 min. The reaction mixture was put in an oil bath at 75ºC. Then 0.44 mmol dissolved in 5 mL water AAPH was added to the reaction mixture for the polymerization with a stirring rate of 600 rpm. After 2h, the reaction mixture containing white colored suspension was centrifuged with acetone and water to remove impurities like the monomer, cross-linker, and the initiator (15800 rpm, 2 min, 25ºC), and was then dried.

The Modification of p(HPMA-Cl) Microgels

The dried p(HPMA-Cl) microgel was modified using with TAEA and PEI agents [25]. A certain amount (0.5 g) of dried-p(HPMA-Cl) microgel was dispersed in 10 mL DMF, and either 6.67 mmol

TAEA or 2 mL PEI was added to this mixture [26]. Then the mixtures were then placed in an oil bath at 80ºC and stirred at 400 rpm. After 24 h, the reaction mixtures were taken into room temperature and the modified p(HPMA)-TAEA and p(HPMA)-PEI microgels were collected by centrifugation (24680 rpm, 10 min, 25ºC). The prepared microgels were washed with DMF and ethanol and dried in an oven at 50ºC [25,27].
Characterization of the microgels.

Fourier Transform Infrared Spectra (FT-IR) analysis of the microgels was conducted using a Thermo Scientific Nicolet iS10 (USA) instrument with an ATR apparatus with 4 cm^{-1} resolution between 4000-650 cm^{-1}.

The charges of the synthesized microgels were determined using Zeta potential. The samples were diluted with 0.01 M KNO_3 solution in water. The charges and size of the microgels were measured with a Zeta-Plus Zeta (DLS/ZETA) (Brookhaven Ins. Crop, USA) potential analyzer.

The thermogravimetric behavior of the prepared microgels was determined using a Thermo Gravimetric Analyzer (TGA/DTA) (SII TG/DTA 6300 model, Japan). Approximately 4-6 mg of dried samples were placed in ceramic crucibles and heated up to 1000ºC from 50ºC under Argon atmosphere with 100 mL min^{-1} flow rate at 2, 6 and 10ºC min^{-1} heating rate.

Thermal Kinetic Analysis

The activation energy is calculated via thermogravimetric data by the following equations' (Equation 1-3): ()
where, A is the frequency factor, E_a is the activation

$$k = Ae^{\left(-E^a/RT\right)}$$ Equation 1

energy (J mol^{-1}), R is the ideal gas constant (3.814 J mol^{-1} K^{-1}), and T is the temperature (K).

Kinetic parameters can be obtained from experiments using different methods as described below. For all these kinetic methods, conversion rate (reaction rate) is a linearly dependent conversion function (α) of the temperature-dependent rate constant (k), whereas it is independent of temperature [2,22,

$$\alpha = \frac{w_0 - w_t}{w_0 - w_\infty}$$ Equation 2

28], and is calculated with the below equation:
where, W_0, W and W_∞ refer to initial, instantaneous, and the final weights, respectively.

Another parameter to calculate the activation

$$\mathrm{k} = \frac{\text{”}\,\mathrm{W}}{\text{”}\,\mathrm{txW}}$$ Equation 3

energy and exponential factor is the heating rate (β in °C/min) and it depends on temperature and time as the following equation:

Solid-state kinetic methods can be classified

$$\beta = \frac{dT}{dt}$$ Equation 4

into two types: experimental (isothermal and non-isothermal) and computational (model-fitting and model-free) methods. Computational methods are also divided into two sub-groups as isothermal (conventional) and non-isothermal (differential) (1).

Kissinger-Akahira-Sunose (KAS) methods

$$\ln\frac{^2}{\mathrm{T}^2} = \ln\frac{\mathrm{AR}}{\mathrm{g}(\mathrm{x})} - \frac{\mathrm{Ea}}{\mathrm{RT}}$$ Equation 5

can provide information about activation energy of solid-state reactions without knowledge of the reaction mechanism.

These method has been applied in the determination of activation energies more extensively than any other multiple-heating rate method [15,29]. A plot of ln β $(T^2)^{-1}$ versus 1 T^{-1} at each yields E_a from the slope for each α of the model.

Flynn-Wall-Ozawa [21] (FWO) method developed independently by Ozawa and Flynn Wall is used to calculate the non-isothermal data. This method can be used to determine the activation energy without the need to know the reaction order or the decomposition mechanism[18,30-34]. The plot of log β against 1 T^{-1} under given value E_a is:

A plot of log β or ln β versus 1 T^{-1} at each α yields

$$\ln^2 = \log\frac{\mathrm{AEa}}{\mathrm{g}(\mathrm{x})}5.331 - 1.502\frac{\mathrm{Ea}}{\mathrm{RT}}$$ Equation 6

E_a from the slope for each α of the model.

Coast-Redfern method is an integral method

$$\log^2 = \log\frac{AEa}{g(x)} 2.315 - 0.457\frac{Ea}{RT}$$ Equation 7

that postulates various orders of reaction and compares the linearity in each case to select the correct order [6,20,32,34]. The activation energy (E_a) constant heating rate for each α, in the plot of ln (β (T_{max}^2)$^{-1}$) versus 1 T^{-1} the slope gives $-E_a R^{-1}$.

The Ozawa method is used to calculate the non-isothermal data [11,21,30]. The plot of log β against 1 T^{-1} under given value E_a is:

Using the Friedman method, the activation energy (E_a) constant heating rate for each α, in the plot of ln [β (T_{max}^2)$^{-1}$] versus 1 T_{max}^{-1} the slope gives $-E R^{-1}$ [19,22,27,34,35]

$$\ln\frac{T^2}{AR} = \ln\left[\frac{Ea}{AR}\left(1-\left(\frac{2AR}{Ea}\right)\right)\right] - \frac{Ea}{RT}$$ Equation 8

$$\log\beta = \log\frac{AE_a}{g(\alpha)} - 1.052\frac{E_a}{RT}$$ Equation 9

$$\ln\frac{d\alpha}{dT} = \ln Ag(\alpha) * e^{-Ea/RT}$$ Equation 10

RESULTS and DISCUSSION

Characterization of the Microgels

P(HPMA-Cl) microgel synthesis and their modification with TAEA and PEI are shown in Figure 1(a). SFEP method was used in p(HPMA-Cl) microgel synthesis, and EGDMA and AIBA were used as the cross-linker and the initiator, respectively. Following this step, p(HPMA)-TAEA and p(HPMA)-PEI microgels were prepared from p(HPMA-Cl) microgels at 80°C. The SEM image of the prepared p(HPMA-Cl) is shown in Figure

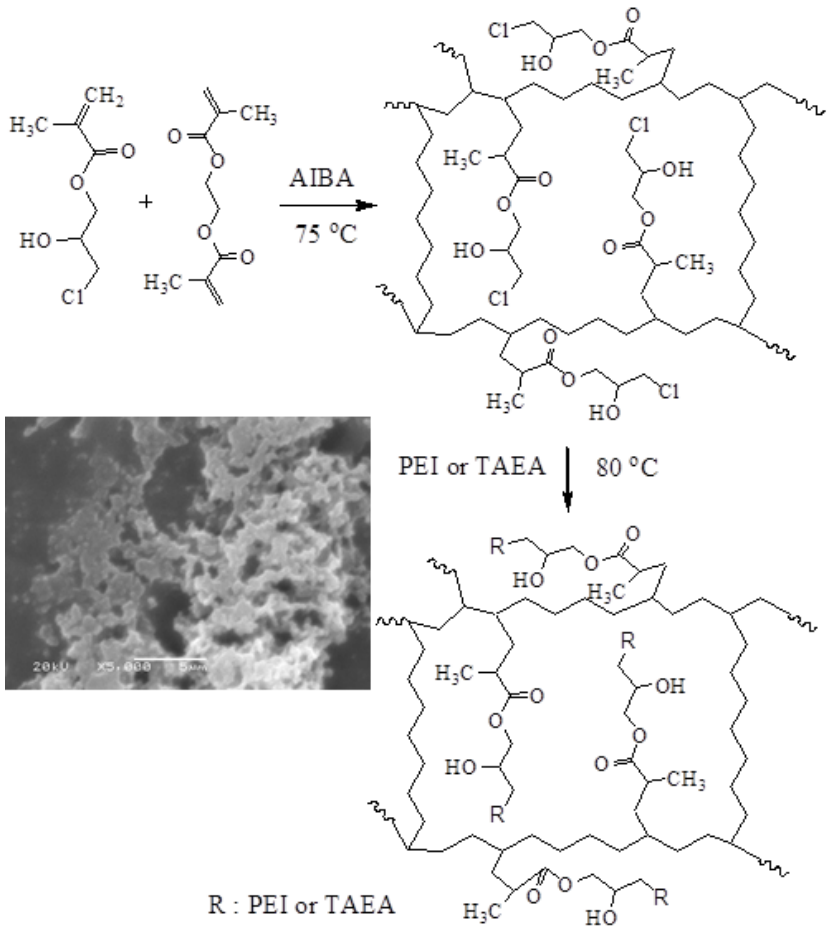

Figure 1. (a) The schematic demonstration of synthesis p(HPMA-Cl) microgels and its modification with PEI or TAEA and **(b)** the SEM images of p(HPMA-Cl) microgels.

1(b). In figure 1(b), it can be seen that the surface of microgels is not smooth. This formation may have originated from the molecule structure of modified agents.

The FT-IR spectra of p(HPMA-Cl), p(HPMA)-TAEA and p(HPMA)-PEI are presented in Figure 2. The characteristic –OH absorption band of p(HPMA-Cl) microgels can be observed between 3600-3000 cm^{-1}. It is evident that the absorption bands at 2955, 1717, 1149 and 704 cm^{-1} are for O–H, aliphatic C–H, C=O, C–O and C–Cl, respectively. In the spectrum of p(HPMA)-TAEA microgels, the band between 3600-3100 cm^{-1} for N–H stretching vibration, the bands at 2924 and 2851 cm^{-1} for C–H stretching vibration and the band at 1656 cm^{-1} for the modification peak (quarternize N-H peak) can be observed. Similarly, the band between 3600-3100 cm^{-1} for N–H stretching vibration, the bands at 2937 and 2834 cm^{-1} for C–H stretching vibration and the band at 1652 cm^{-1} for the modification peak (quarternize N-H peak) can be observed in the spectrum of p(HPMA)-PEI microgels. After the modification of p(HPMA-Cl) microgels with TAEA and PEI, the specific C–Cl absorption band at 704 cm^{-1} was found to have disappeared in the spectra for p(HPMA)-TAEA and p(HPMA)-PEI. Additionally, the modification peak (quarternize N-H peak) in spectra of p(HPMA)-TAEA and p(HPMA)-PEI [36] can be seen clearly. The modification peak and disappearance of the specific C–Cl absorption band are clear indicators that the modification reaction of p(HPMA-Cl) microgels with TAEA and PEI have occurred.

Table 1 shows the DLS results for three different microgels: p(HPMA-Cl), p(HPMA)-TAEA and p(HPMA)-PEI. The hydrodynamic diameters of the p(HPMA-Cl), p(HPMA)-TAEA and p(HPMA)-PEI microgels were measured as 595 ± 12, 758 ± 55 and 899±32 nm by DLS. After p(HPMA-Cl) microgels were modified with TAEA or PEI, the hydrodynamic diameters of the modified p(HPMA)-TAEA and p(HPMA)-PEI microgels were found to have increased approximately by 20-35%. The swelling

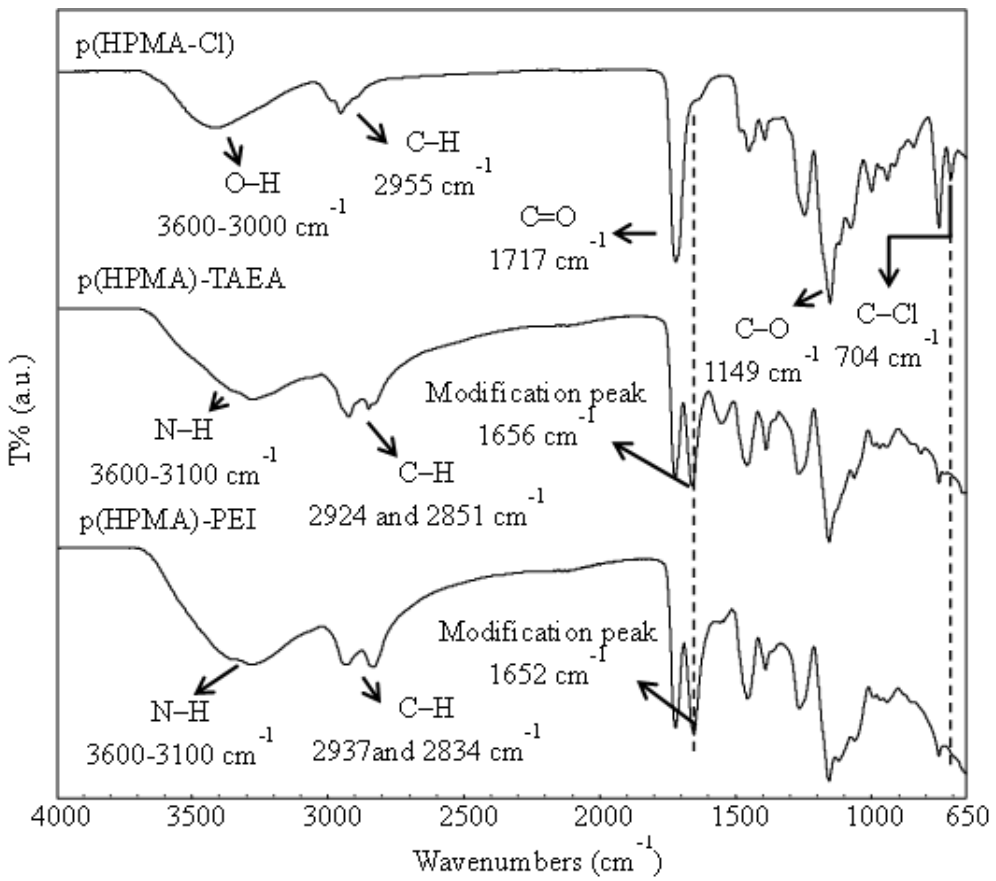

Figure 2. FT-IR spectra of p(HPMA-Cl), p(HPMA)-TAEA and p(HPMA)-PEI.

Table 1. The DLS and ζ-potential measurements of the prepared microgels.

Microgel	DLS* (nm)	Zeta Potential* (mV)
p(HPMA-Cl)	595±12	39.6±3.7
P(HPMA)-TAEA	758±55	23.0±1.0
P(HPMA)-PEI	899±32	15.6±0.8

of modified microgels p(HPMA)-TAEA and p(HPMA)-PEI were related with their quarternized amine groups. The amine groups in p(HPMA)-TAEA and p(HPMA)-PEI microgels were formed as hydrogen bonded with DI water, which causes the swelling of prepared modified microgels. The ζ-potentials of the p(HPMA-Cl), p(HPMA)-TAEA and p(HPMA)-PEI microgels were measured as 39.6±3.7, 15.6 ± 0.8 and 23.0±1.0 respectively, and are shown in Table 1. The ζ-potential results for p(HPMA)-TAEA and p(HPMA)-PEI microgels were positive due to their surfaces having been formed of quarternized amines.

Thermal Kinetic Analysis

The kinetics parameters related to the degradation reactions of the p(HPMA-Cl)-based microgels were determined by TGA-DTA experimental results.

The temperature was linearly increased with the heating rates of 2, 6, and 10 °C min^{-1}. Figs. 3 to 5 show the thermogravimetric curves of p(HPMA-Cl), p(HPMA)-TAEA and p(HPMA)-PEI microgels (under an inert atmosphere at heating rates ranging as 2, 6 and 10°C min^{-1}). As can be seen in the figures, the difference in the degradation process between microgels was particularly

Table 2. Decomposition characteristics of p(HPMA-Cl), p(HPMA)-PEI and p(HPMA)-TAEA) microgels with different heating rates.

Heat rate	Stages of degradation	Temperature range	Maximum peak	Loss of mass
		p(HPMA-Cl)		
2 (K/min)	1st stage	224°C-467°C	338°C	91%
6 (K/min)	1st stage	229°C-462°C	317°C	91%
10 (K/min)	1st stage	243°C-445°C	36 °C	91%
		p(HEMA)-PEI		
2 (K/min)	1st stage	315°C-390°C	319°C	62%
	2nd stage	400°C-488°C	399°C	83%
6 (K/min)	1st stage	316°C-390°C	344°C	56%
	2nd stage	400°C-420°C	410°C	83%
10 (K/min)	1st stage	293 °C-356°C	346°C	41%
	2nd stage	360°C-402°C	421°C	83%
		p(HEMA)-TAEA		
2 (K/min)	1st stage	284°C-321°C	302°C	39%
	2nd stage	400°C-468°C	393°C	95%
6 (K/min)	1st stage	279°C-350°C	306°C	40%
	2nd stage	389°C-502°C	420°C	95%
10 (K/min)	1st stage	286°C-340°C	313°C	34%
	2nd stage	378°C-552°C	394°C	95%

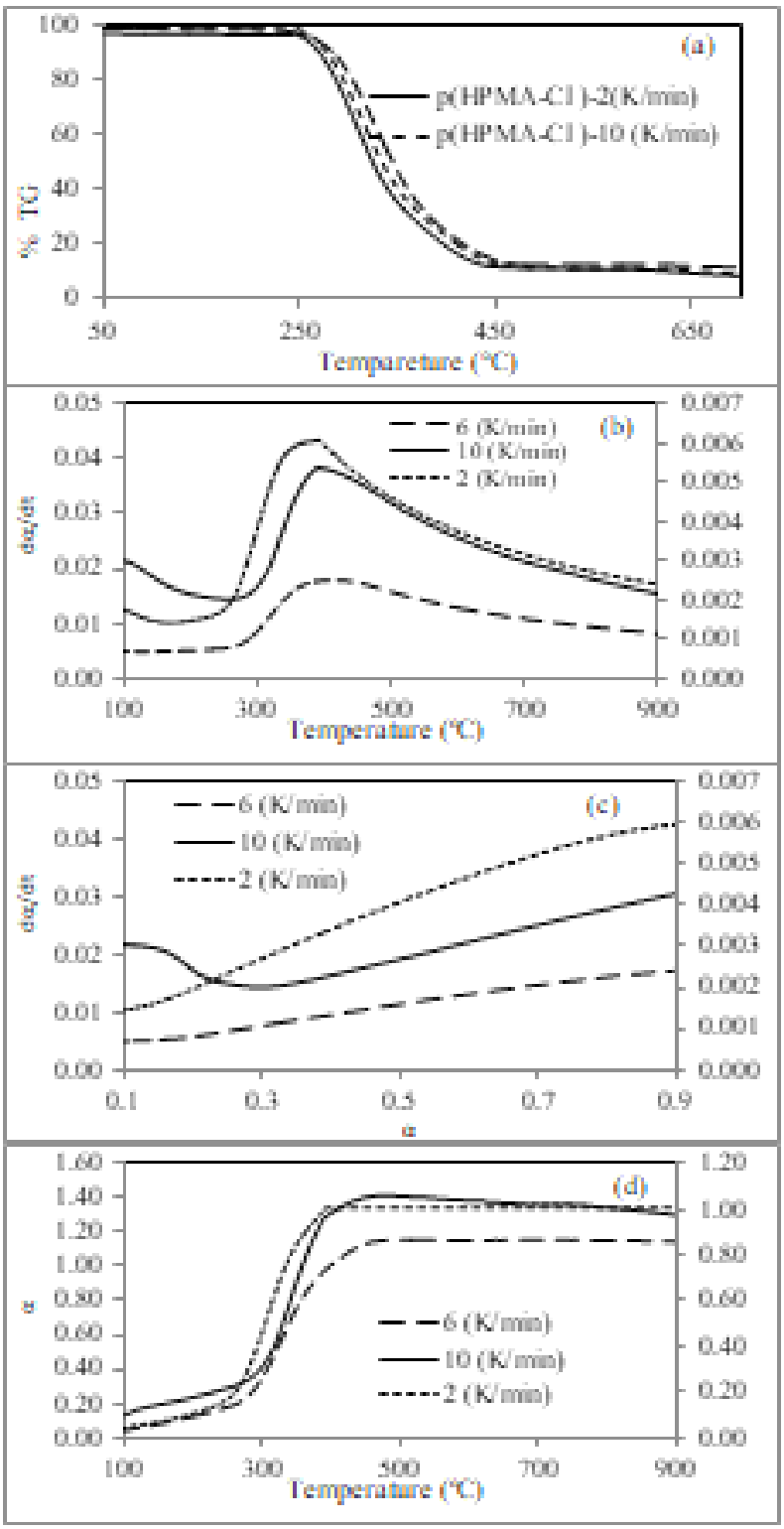

Figure 3. The p(HPMA-Cl) microgel of (a) Thermogram experimental curve (b) DTG experimental curve (c) comparison of the degradation rate curves given as a function of conversion and (d) Experimental normalized integral and DTG curves (DTG curves as an inset) obtained for the thermal decomposition (linear heating rate of 2, 6 and 10°C/ min).

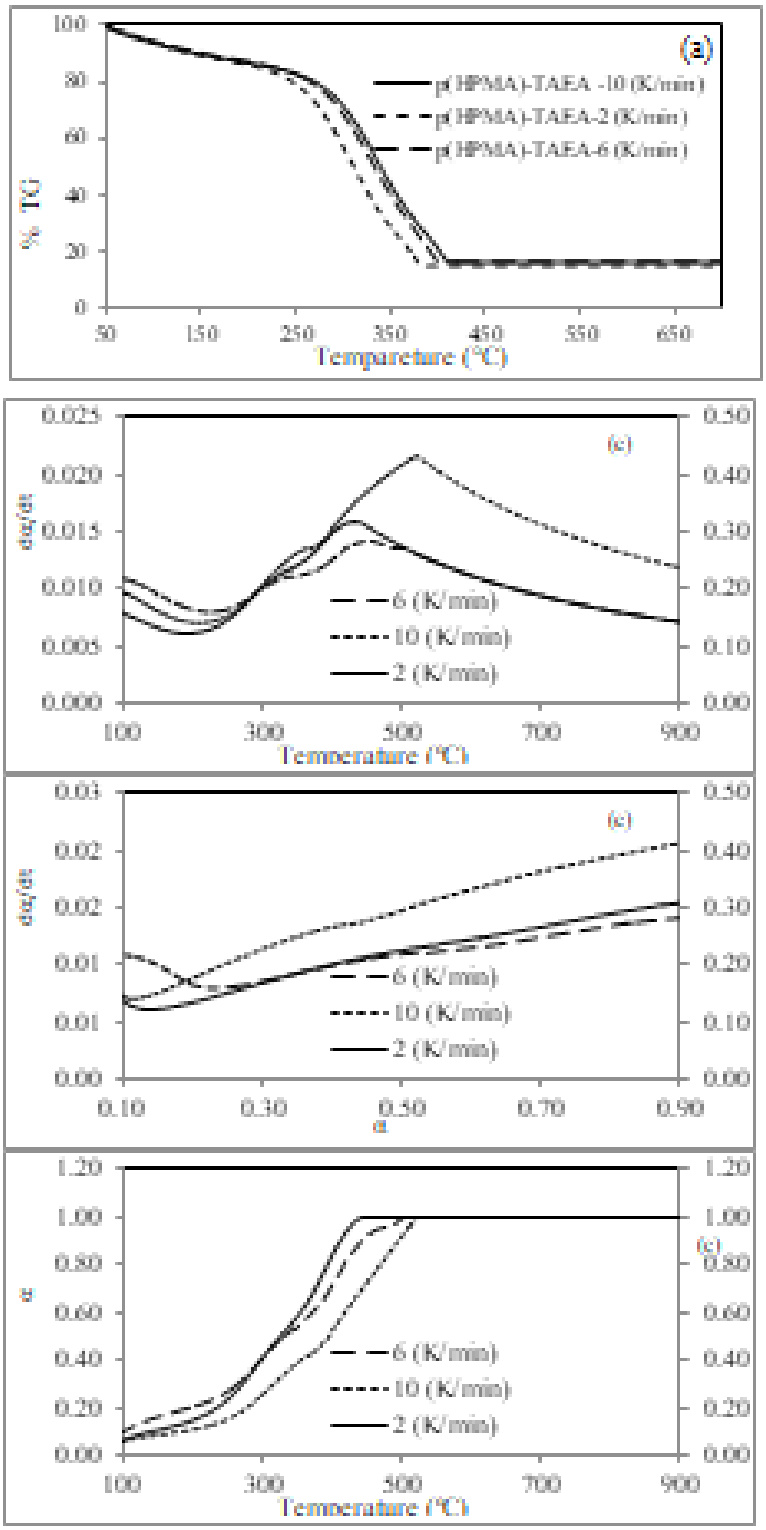

Figure 4. The p(HPMA-Cl)-ITAEA microgel of (a) Thermogram experimental curve (b) DTG experimental curve (c) comparison of the degradation rate curves given as a function of conversion and (d) Experimental normalized integral and DTG curves (DTG curves as an inset) obtained for the thermal decomposition (linear heating rate of 2, 6 and 10°C/ min).

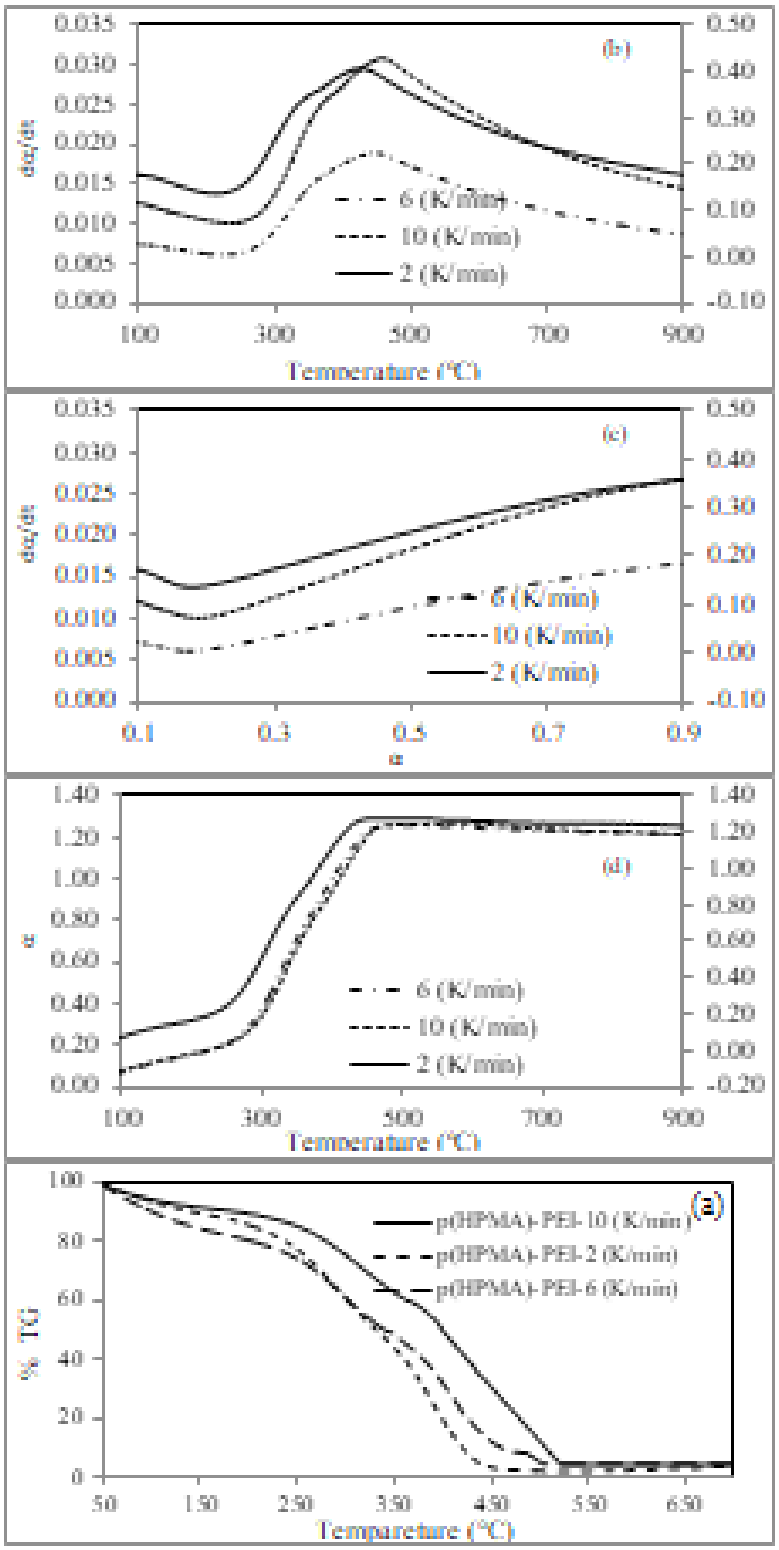

Figure 5. The p(HPMA-Cl)-PEI microgel of (a) Thermogram experimental curve (b) DTG experimental curve (c) comparison of the degradation rate curves given as a function of conversion and (d) Experimental normalized integral and DTG curves (DTG curves as an inset) obtained for the thermal decomposition (linear heating rate of 2, 6 and 10°C/ min).

observable in the shape of the derivative thermosgravimetric (DTG) curves. The side peak at lower temperatures associated with water evaporation is also distinguishable. It appears that some water wasn't removed at the first stage of degradation, and its elimination reactions began at very low temperatures. Microgels begin to decompose and the decomposition temperature seems to be increasing as the heating rate is around 250°C.

The experimental TGA analysis of p(HPMA-Cl), p(HPMA)-TAEA and p(HPMA)-PEI microgels reveal different stability levels. The evolution of the rate of mass loss ($d\alpha\ dt^{-1}$) of unmodified of p(HPMA-Cl), p(HPMA)-TAEA and p(HPMA)-PEI by temperature are shown in Figure 4-6. The decomposition stage temperature and percent loss of mass thermal degradation for p(HPMA-Cl), p(HPMA)-TAEA and p(HPMA)-PEI microgels are summarized in Table 2. It is the natural expectation that the increase of p(HPMA-Cl) content and the presence of crosslinks should increase the stability of the microgel. Nevertheless, it was reported for p(HPMA-Cl) microgels that the hydroxyl and amine groups contribute to the stiffness of the polymer via hydrogen bonding. When the number of amine groups was diminished by crosslinking, the hydrogen bonding was attenuated and the stiffness was found to have diminished. This is due to the fact that the crosslinked structures induce less stiffness compared to the hydrogen bonding [11]. Consequently, the stability of crosslinked p(HPMA-Cl), p(HPMA)-TAEA and p(HPMA)-PEI microgels were a compromise between two effects: crosslink density and hydrogen bond interactions of amine and hydroxyl groups. As can be seen in Figures 4-6, these degradation reactions in the p(HPMA-Cl) microgel had occurred at very low temperatures compared to the p(HPMA)-TAEA and p(HPMA)-PEI microgels. The advance of the DTG peaks may be caused by the increasing amine content. This fact was also observed in Figures 3-5, where the degradation rate was given as a function of degradation conversion.

The p(HPMA-Cl), p(HPMA)-TAEA and p(HPMA)-PEI microgels were subjected to different heating rates (2, 6, 10°C min^{-1}). The alteration of the rate of mass loss ($d\alpha\ dt^{-1}$) of the p(HPMA-Cl), p(HPMA)-TAEA and p(HPMA)-PEI microgels with temperature was shown in Figure 4-6. These degradation reactions in the p(HPMA-Cl) microgel occurred at very low temperatures with respect to the modified p(HPMA)-TAEA and p(HPMA)-PEI microgels (Figure 3c-5c). As conversion increases, a similar trend described for modified p(HPMA)-TAEA and p(HPMA)-PEI microgels can be observed.

In order to determine the reaction mechanism involved during the process of the thermal degradation of microgels, 24 types of reaction mechanisms were tested. Model derivation was based on the suggested reaction mechanisms (nucleation, diffusion, geometric shape, and reaction order). In order to understand the kinetic variance and reaction mechanism functions, the integral to differential equations for microgels was solved and compared with the experimental data.

Nucleation and Nuclei Growth Models (A, B, P, Prout and Tompkins) reactions contain decomposition, hydration, crystallization, crystallographic transition, adsorption, and desolation [3, 4, 14, 15]. Geometrical contraction (R) models postulate that nucleation occurs quickly on the surface of the crystal. The rate of decomposition was controlled by the resulting reaction interface proceeding toward the center of the crystal. Order-based (F) models were the simplest models as they resemble those used in homogeneous kinetics [1, 31, 32].

It can be seen from figure 6-8 that reaction mechanisms include reaction order, geometric shape, diffusion, and nucleation. Every stage for the thermal degradation microgels was calculated, down to the decomposition correlation coefficient and mechanisms.

Thermogravimetric degradations of the microgels were also investigated and compared using four different methods. These methods are as follows:

*for each α (0.1-0.9), in the plot of α versus t shapes gives model fit.

*for each α (0.1-0.9), in the plot of $d\alpha\ dt^{-1}$ versus α

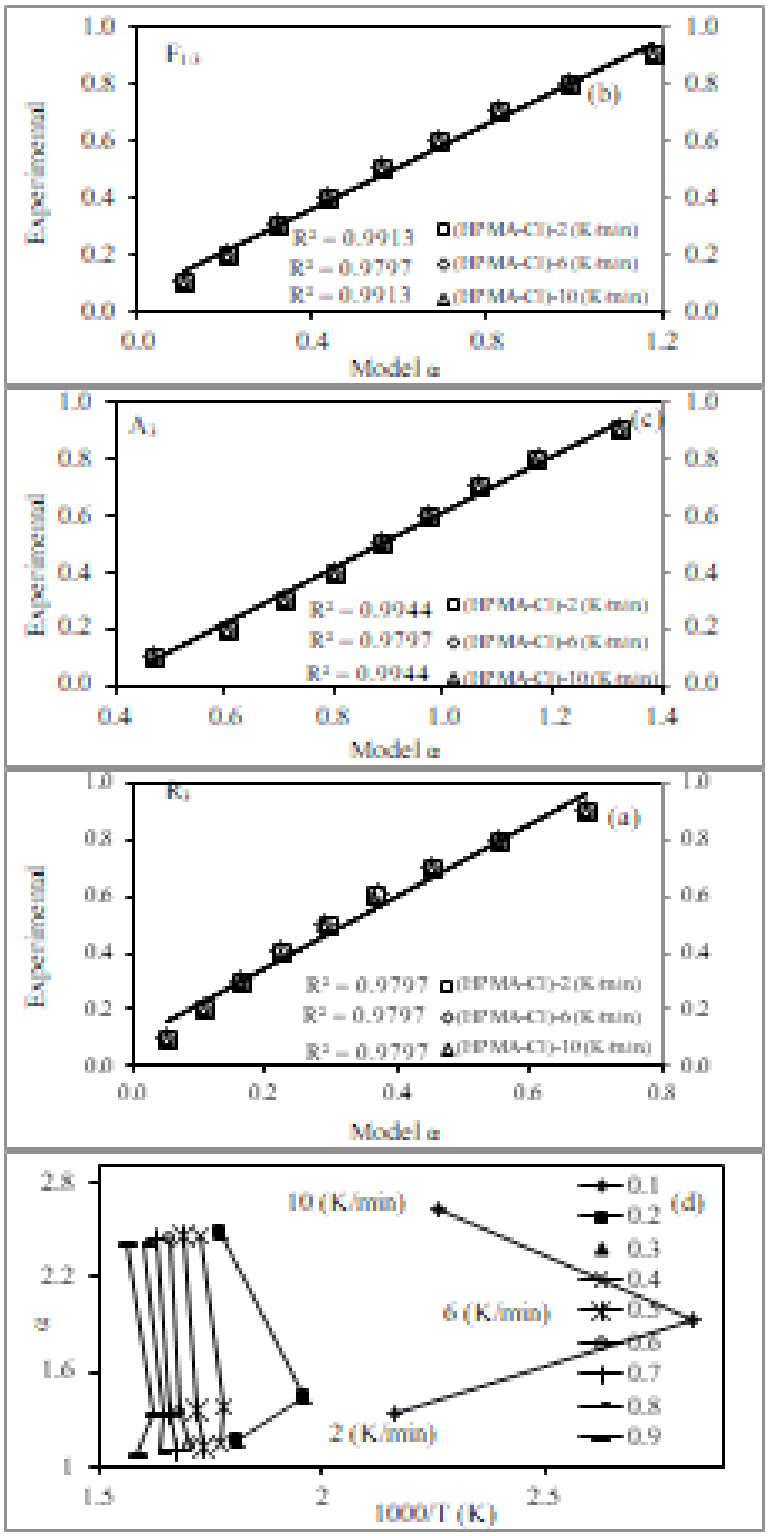

Figure 6. The thermal degradations (a) Order-based (F), (b) Geometrical contraction (R), (c) Nucleation and Nuclei Growth (A) models model and correlation coefficient (d) Friedman plots resulting of the isoconversional of p(HPMA-Cl) microgel.

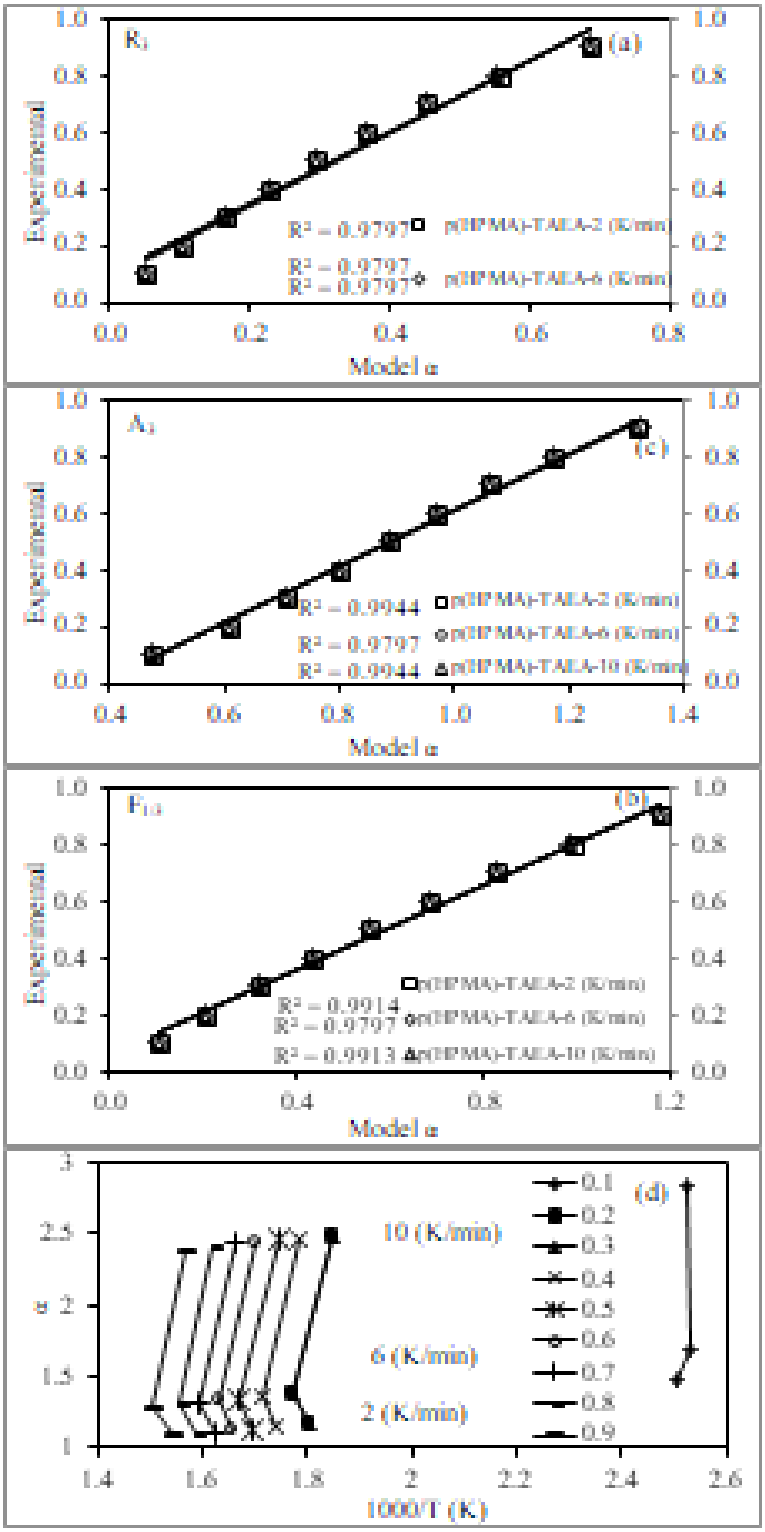

Figure 7. The thermal degradations (a) Order-based (F), (b) Geometrical contraction (R), (c) Nucleation and Nuclei Growth (A) models and correlation coefficient of (d) Friedman plots resulting of the isoconversional of p(HPMA)-TAEA) microgel.

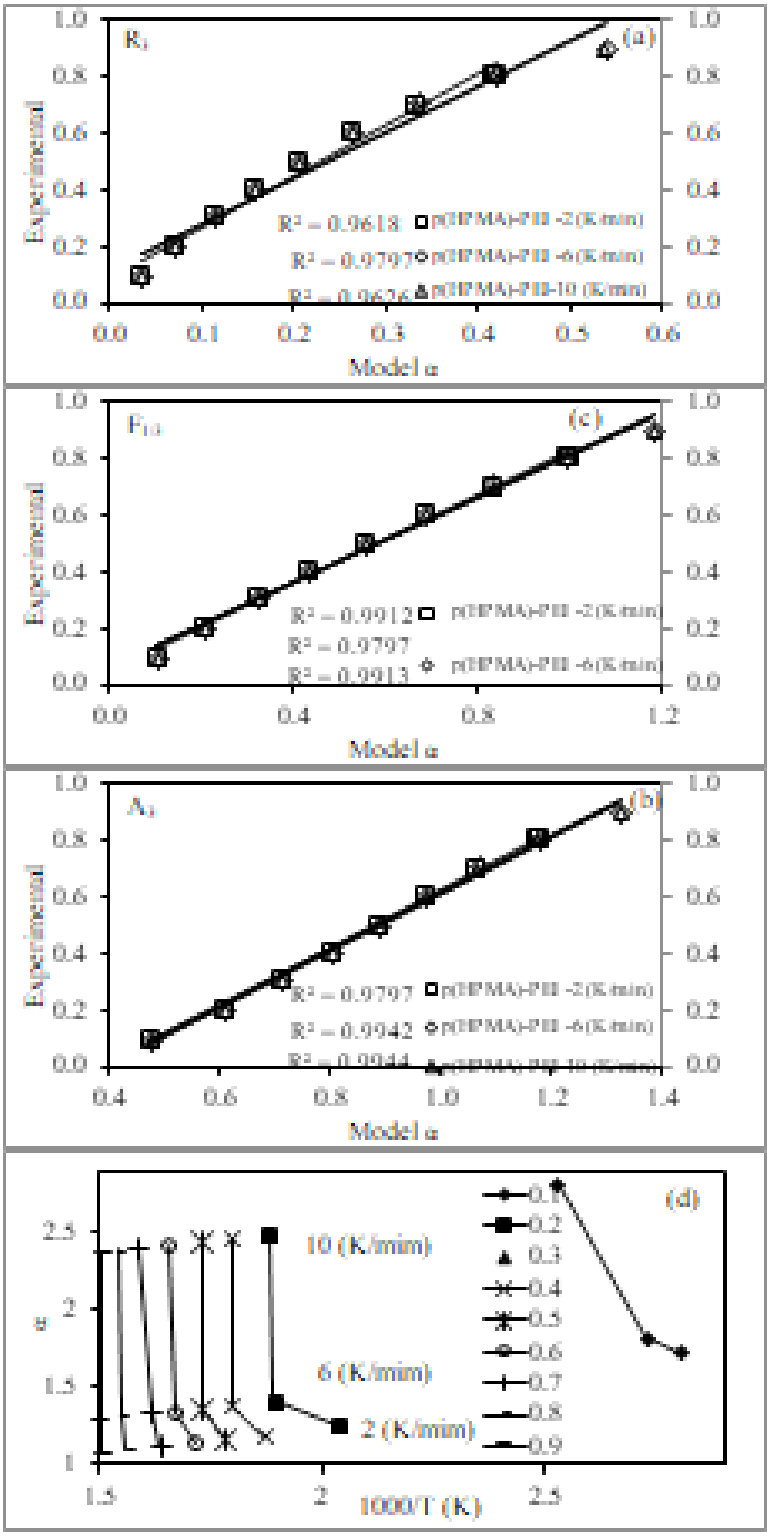

Figure 8. The thermal degradations (a) Order-based (F), (b) Geometrical contraction (R), (c) Nucleation and Nuclei Growth (A) models and correlation coefficient (d) Friedman plots resulting of the isoconversional of of p(HPMA)-PEI microgel.

shapes gives model fit.

*for each model, in plot of α (0.1-0.9) versus temperature shapes gives model fit.

*for each α (0.1-0.9), in the plot experimental α versus model α gives correlations. This correlation is related to the model fit.

The p(HPMA-Cl), p(HPMA)-TAEA and p(HPMA)-PEI microgels were decomposed over four stages (Figure 6 a-c), three stages (Figure 7a-c) and four (Figure 8 a-c) stages respectively, and at different temperatures. F, R, and A models of the thermal degradation models of the microgels were more suitable compared to the other models. The correlation coefficient of values above mentioned was obtained using experimental/models graphs for comparison. These correlation coefficient values thus indicated which model was most suitable related to them. The similarity of the thermal degradation kinetics of p(HPMA-Cl), p(HPMA)-TAEA and p(HPMA)-PEI microgels were explained with reaction order and geometric shape model as that mechanism functions.

The conversion value (α) was calculated from the TGA data for each temperature step according to kinetic parameters as with Kissinger-Akahira Sunose (KAS) [5], Flynn-Wall-Ozawa (FWO) [12], Coats-Redfern[7,29], Ozawa [12,24] and Friedman [12] methods. The kinetic analysis of the TG-DTG curve was calculated by means of Equation 6-11 [22,32,33]. The degradation reaction activation energy correlations of p(HPMA-Cl), p(HPMA)-TAEA and p(HPMA)-PEI microgels were summarized in Table 3.

The thermal decomposition of p(HPMA-Cl), p(HPMA)-TAEA and p(HPMA)-PEI microgels were found to be suitable for D_1, $F_{1/3\text{-}0\ (n:3\text{-}0)}$, $R_{3\text{-}1,}$ $B_{1,}$ $A_{3\text{-}4}$ and P_2 models. As can be seen from Table 3-5, the activation energy value calculations for microgels were model-dependent. Geometrical contraction (R_3) model has the lowest activation energy with 6.03 J mol^{-1} K^{-1}, 2.63 J mol^{-1} K^{-1}, and 3.11 J mol^{-1} $K^{-1}$for p(HPMA-Cl), p(HPMA)-TAEA and p(HPMA)-PEI microgels, respectively. While the model-independent thermal decomposition calculations for p(HPMA-Cl) gave the lowest activation energy (10°C min^{-1}, 6.3 J mol^{-1} K^{-1}) with Kissinger-Akahira Sunose (KAS) model, the p(HPMA)-TAEA and p(HPMA)-PEI have the lowest activation energy levels of 10.09 J mol^{-1} K^{-1} (6°C min^{-1}) and 9.8 J mol^{-1} K^{-1} (10 °C min^{-1}) for Coats-Redfern model, respectively. The activation energy value for microgels (2, 6, 10°C min^{-1}) were calculated to be model-independent for the Kissinger-Akahira Sunose (KAS), Flynn-Wall-Ozawa (FWO), Coats-Redfern, Ozawa and Friedman (Table 3) methods.

Figure 6d-8d shows the activation energies of p(HPMA-Cl), p(HPMA)-TAEA and p(HPMA)-PEI microgels from Friedman plot for selected some values of microgels. The values of the activation energy for each alpha were calculated from the slope plots for the different α conversions. For α> 0.1 the activation energy was considerably higher due to chain scission reactions. For the Kissinger-Akahira Sunose (KAS), Flynn-Wall-Ozawa (FWO), Coats-Redfern, Ozawa and Friedman methods, kinetic models were not accepted due to the calculated activation energies being negative. The activation energy data produced using the Kissinger-Akahira Sunose (KAS), Flynn-Wall-Ozawa (FWO), Coats-Redfern, Flynn-Wall-Ozawa methods showed variations. These variations are plausible owing to the temperature change that was used in nonlinear isothermal kinetic methods. In addition, p(HPMA-Cl), p(HPMA)-TAEA and p(HPMA)-PEI microgels may have resulted from the degradation process by multistep kinetic mechanisms, which is evident in the nonlinear relationship between the activation energy and the conversion rate. The thermal degradation analysis shows that the activation energy varies with the conversion degree as a consequence of multiphase reactions, and the physical changes that the reactions produced in the modified microgels.

CONCLUSION

In this study, isoconversion kinetic analysis methodology was applied to investigate the thermal degradation of p (HPMA-Cl) microgels modified with TAEA and PEI modifier agents. No significantly different behaviors were observed any of the samples, including the basic thermal degradation mechanism, the elimination of side groups (hydroxyl groups, amine) from the main chain, and the formation of water and conjugated and non-conjugated polymer structures. It was

Table 3. Activation energy values for p(HPMA-Cl), p(HPMA)-PEI and p(HPMA)-TAEA microgels were calculated model-independent.

Microgels	p(HPMA-Cl)		p(HPMA)-PEI		p(HPMA)-TAEA	
Kinetics Model	R^2	Ea (J/mol K)	R^2	Ea (J/mol K)	R^2	Ea (J/mol K)
KAS	0.9305	44.15	0.9314	31.26	0.9169	22.37
FWO	0.9983	-4.73	0.9930	-4.07	0.9955	-4.63
Coast-Redfern	0.8866	34.75	0.7250	20.70	0.7250	12.14
Ozawa	0.9983	-2.05	0.9980	-1.75	0.9955	-2.00
Friedman	0.9120	-39.33	0.8968	-25.94	0.8552	-17.21

Table 4. Activation energy of values for p(HPMA-Cl) microgel were calculated model-dependent.

	p(HPMA-Cl) (2 K/min)					p(HPMA-Cl) (6 K/min)					p(HPMA-Cl) (10 K/min)				
Model	KAS (J/mol K)	FWO (J/mol K)	Coast-Redfern (J/mol K)	Ozawa (J/mol K)	Freidman (J/mol K)	KAS (J/mol K	FWO (J/mol K)	Coast-Redfern (J/mol K)	Ozawa (J/mol K)	Freidman (J/mol K)	KAS (J/mol K	FWO (J/mol K)	Coast-Redfern (J/mol K)	Ozawa (J/mol K)	Freidman (J/mol K)
D1	11.47	25.11	11.47	10.85	11.47	8.6	18.7	8.6	8.1	8.6	4.03	8.82	4.03	3.81	4.03
D2	8.90	19.47	8.90	8.42	8.90	6.4	14.0	6.4	6.1	6.4	3.01	6.59	3.01	2.85	3.01
D3	-3.41	-7.46	-3.41	-3.22	-3.41	2.4	5.2	2.4	2.3	2.4	-1.11	-2.44	-1.11	-1.05	-1.11
D4	2.38	5.20	2.38	2.25	2.38	1.7	3.7	1.7	1.6	1.7	0.79	1.73	0.79	0.75	0.79
F0	12.35	27.02	12.35	11.68	12.35	9.3	20.4	9.3	8.8	9.3	4.67	10.22	4.67	4.42	4.67
F1	28.96	63.37	28.96	27.40	28.96	21.1	46.2	21.1	20.0	21.1	9.98	21.83	9.98	9.44	9.98
F1/3	15.91	34.82	15.91	15.05	15.91	11.9	26.0	11.9	11.2	11.9	5.86	12.82	5.86	5.54	5.86
F1/2	18.26	39.95	18.26	17.27	18.26	13.6	29.7	13.6	12.8	13.6	-6.62	-14.48	-6.62	-6.26	-6.62
F2/3	31.83	69.65	31.83	30.11	31.83	23.9	52.2	23.9	22.6	23.9	11.72	25.65	11.72	11.09	11.72
F2	94.30	206.35	94.30	89.21	94.30	66.0	144.5	66.0	62.5	66.0	28.85	63.13	28.85	27.29	28.85
F3	874.69	1913.9	874.69	827.44	874.69	590.3	1291.7	590.3	558.4	590.3	242.20	529.98	242.20	229.12	242.20
R1	12.35	27.02	12.35	11.68	12.35	9.3	20.4	9.3	8.8	9.3	4.67	10.22	4.67	4.42	4.67
R2	9.13	19.98	9.13	8.64	9.13	6.8	14.9	6.8	6.4	6.8	3.31	7.24	3.31	3.13	3.31
R3	7.03	15.39	7.03	6.65	7.03	5.2	11.4	5.2	4.9	5.2	2.51	5.49	2.51	2.37	2.51
B1	63.83	139.67	63.83	60.38	63.83	48.9	107.0	48.9	46.2	48.9	24.03	52.58	24.03	22.73	24.03
B2	58.05	127.03	58.05	54.92	58.05	40.7	89.0	40.7	38.5	40.7	17.71	38.75	17.71	16.75	17.71
B3	116.41	254.73	116.41	110.12	116.41	79.5	173.9	79.5	75.2	79.5	32.93	72.05	32.93	31.15	32.93
A2	17.14	37.50	17.14	16.21	17.14	12.9	28.2	12.9	12.2	12.9	6.31	13.81	6.31	5.97	6.31
A3	12.47	27.29	12.47	11.80	12.47	9.5	20.7	9.5	9.0	9.5	4.69	10.26	4.69	4.44	4.69
A4	9.84	21.52	9.84	9.30	9.84	7.5	16.5	7.5	7.1	7.5	4.15	9.08	4.15	3.92	4.15
A5	21.28	46.56	21.28	20.13	21.28	15.8	34.6	15.8	14.9	15.8	7.66	16.76	7.66	7.24	7.66
P2	9.97	21.81	9.97	9.43	9.97	7.7	16.9	7.7	7.3	7.7	3.91	8.57	3.91	3.70	3.91
P3	-7.93	-17.36	-7.93	-7.50	-7.93	6.1	13.4	6.1	5.8	6.1	3.14	6.88	3.14	2.97	3.14
P4	6.52	14.26	6.52	6.17	6.52	5.1	11.2	5.1	4.8	5.1	-5.17	-11.32	-5.17	-4.89	-5.17

Table 5. Activation energy of values for p(HPMA)-PEI microgel were calculated model-dependent.

	p(HPMA)-PEI (2 K/min)					p(HPMA)-PEI (6 K/min)					p(HPMA)-PEI (10 K/min)				
Model	KAS (J/mol K	FWO (J/mol K)	Coast-Redfern (J/mol K)	Ozawa (J/mol K)	Freidman (J/mol K)	KAS (J/mol K)	FWO (J/mol K)	Coast-Redfern (J/mol K)	Ozawa (J/mol K)	Freidman (J/mol K)	KAS (J/mol K)	FWO (J/mol K)	Coast-Redfern (J/mol K)	Ozawa (J/mol K)	Freidman (J/mol K)
D1	5.37	11.75	5.37	5.08	5.37	5.93	12.97	5.93	5.61	5.93	5.38	11.77	5.38	5.09	5.38
D2	3.89	8.51	3.89	3.68	3.89	4.52	9.90	4.52	4.28	4.52	4.08	8.93	4.08	3.86	4.08
D3	1.35	2.95	1.35	1.27	1.35	1.72	3.77	1.72	1.63	1.72	1.55	3.38	1.55	1.46	1.55
D4	1.00	2.18	1.00	0.94	1.00	1.20	2.62	1.20	1.13	1.20	1.08	2.37	1.08	1.02	1.08
F0	6.35	13.90	6.35	6.01	6.35	6.66	14.57	6.66	6.30	6.66	6.09	13.34	6.09	5.77	6.09
F1	12.64	27.65	12.64	11.96	12.64	14.88	32.57	14.88	14.08	14.88	13.47	29.47	13.47	12.74	13.47
F1/3	7.85	17.17	7.85	7.42	7.85	8.40	18.38	8.40	7.94	8.40	-8.31	-18.19	-8.31	-7.87	-8.31
F1/2	8.73	19.10	8.73	8.26	8.73	9.64	21.10	9.64	9.12	9.64	8.73	19.10	8.73	8.26	8.73
F2/3	15.71	34.39	15.71	14.87	15.71	16.96	37.12	16.96	16.05	16.96	15.38	33.66	15.38	14.55	15.38
F2	29.77	65.13	29.77	28.16	29.77	46.48	101.70	46.48	43.97	46.48	41.24	90.24	41.24	39.01	41.24
F3	167.12	365.69	167.12	158.09	167.12	42.15	92.24	42.15	39.88	42.15	36.42	79.69	36.42	34.45	36.42
R1	6.35	13.90	6.35	6.01	6.35	6.66	14.57	6.66	6.30	6.66	6.09	13.32	6.09	5.76	6.09
R2	4.39	9.61	4.39	4.15	4.39	4.81	10.53	4.81	4.55	4.81	4.38	9.59	4.38	4.15	4.38
R3	3.28	7.19	3.28	3.11	3.28	3.68	8.06	3.68	3.48	3.68	3.34	7.31	3.34	3.16	3.34
B1	32.18	70.41	32.18	30.44	32.18	34.75	76.05	34.75	32.88	34.75	31.76	69.50	31.76	30.05	31.76
B2	19.37	42.39	19.37	18.33	19.37	28.60	62.59	28.60	27.06	28.60	25.36	55.49	25.36	23.99	25.36
B3	28.85	63.13	28.85	27.29	28.85	55.79	122.08	55.79	52.78	55.79	48.97	107.16	48.97	46.33	48.97
A2	8.31	18.19	8.31	7.87	8.31	9.15	20.01	9.15	8.65	9.15	8.40	18.38	8.40	7.94	8.40
A3	6.29	13.75	6.29	5.95	6.29	6.75	14.77	6.75	6.39	6.75	6.15	13.46	6.15	5.82	6.15
A4	5.04	11.03	5.04	4.77	5.04	5.36	11.73	5.36	5.07	5.36	4.91	10.73	4.91	4.64	4.91
A5	9.98	21.83	9.98	9.44	9.98	11.22	24.56	11.22	10.62	11.22	10.23	22.38	10.23	9.67	10.23
P2	5.37	11.75	5.37	5.08	5.37	5.52	12.08	5.52	5.22	5.52	5.07	11.10	5.07	4.80	5.07
P3	4.33	9.48	4.33	4.10	4.33	4.42	9.68	4.42	4.18	4.42	4.07	8.91	4.07	3.85	4.07
P4	3.58	7.84	3.58	3.39	3.58	3.66	8.01	3.66	3.46	3.66	3.37	7.37	3.37	3.19	3.37

Table 6. Activation energy of values for p(HPMA)-TAEA microgel were calculated model-dependent.

	p(HPMA)-TAEA (2 K/min)					p(HPMA)-TAEA (6 K/min)					p(HPMA)-TAEA (10 K/min)				
Model	KAS (J/molK)	FWO (J/mol K)	Coast-Redfern (J/mol K)	Ozawa (J/mol K)	Freidman (J/mol K)	KAS (J/mol K	FWO (J/mol K)	Coast-Redfern (J/mol K)	Ozawa (J/mol K)	Freidman (J/mol K)	KAS (J/mol K	FWO (J/mol K)	Coast-Redfern (J/mol K)	Ozawa (J/mol K)	Freidman (J/mol K)
D1	6.33	13.86	6.33	5.99	6.33	46.15	100.97	46.15	43.65	46.15	-383.68	-839.55	-383.68	-362.95	-383.68
D2	4.85	10.61	4.85	4.59	4.85	3.46	7.57	3.46	3.27	3.46	-28.76	-62.93	-28.76	-27.21	-28.76
D3	1.85	4.06	1.85	1.75	1.85	1.31	2.87	1.31	1.24	1.31	-10.92	-23.90	-10.92	-10.33	-10.92
D4	1.28	2.80	1.28	1.21	1.28	0.91	2.00	0.91	0.87	0.91	-7.60	-16.64	-7.60	-7.19	-7.60
F0	6.92	15.14	6.92	6.54	6.92	5.01	10.95	5.01	4.73	5.01	-41.62	-91.07	-41.62	-39.37	-41.62
F1	15.71	34.39	15.71	14.87	15.71	10.98	24.02	10.98	10.38	10.98	-91.26	-199.69	-91.26	-86.33	-91.26
F1/3	0.01	19.29	8.81	8.34	8.81	0.01	13.97	6.39	6.04	6.39	9.64	-116.18	-53.09	-50.22	-53.09
F1/2	10.14	22.20	10.14	9.60	10.14	7.28	15.94	7.28	6.89	7.28	-60.56	-132.51	-60.56	-57.29	-60.56
F2/3	17.71	38.75	17.71	16.75	17.71	12.80	28.02	12.80	12.11	12.80	-106.46	-232.96	-106.46	-100.71	-106.46
F2	49.30	107.89	49.30	46.64	49.30	35.00	76.60	35.00	33.11	35.00	-291.04	-636.85	-291.04	-275.32	-291.04
F3	44.07	96.43	44.07	41.69	44.07	312.54	683.90	312.54	295.66	312.54	-2598.6	-5686.2	-2598.6	-2458.2	-2598.6
R1	6.90	15.10	6.90	6.53	6.90	5.01	10.95	5.01	4.73	5.01	-41.62	-91.07	-41.62	-39.37	-41.62
R2	5.06	11.06	5.06	4.78	5.06	3.64	7.97	3.64	3.45	3.64	-30.28	-66.26	-30.28	-28.64	-30.28
R3	3.87	8.48	3.87	3.67	3.87	2.79	6.09	2.79	2.63	2.79	-23.16	-50.68	-23.16	-21.91	-23.16
B1	35.50	77.69	35.50	33.59	35.50	25.69	56.22	25.69	24.30	25.69	-213.61	-467.43	-213.61	-202.08	-213.61
B2	30.51	66.77	30.51	28.87	30.51	21.62	47.30	21.62	20.45	21.62	-179.74	-393.30	-179.74	-170.03	-179.74
B3	59.37	129.90	59.37	56.16	59.37	41.91	91.70	41.91	39.64	41.91	-348.42	-762.41	-348.42	-329.60	-348.42
A2	9.48	20.74	9.48	8.97	9.48	6.85	14.99	6.85	6.48	6.85	-56.96	-124.65	-56.96	-53.89	-56.96
A3	6.94	15.19	6.94	6.57	6.94	5.02	10.99	5.02	4.75	5.02	-41.76	-91.37	-41.76	-39.50	-41.76
A4	5.49	12.01	5.49	5.19	5.49	3.97	8.70	3.97	3.76	3.97	-33.04	-72.31	-33.04	-31.26	-33.04
A5	11.72	25.65	11.72	11.09	11.72	8.48	18.56	8.48	8.02	8.48	-70.51	-154.30	-70.51	-66.70	-70.51
P2	5.62	12.30	5.62	5.32	5.62	4.08	8.93	4.08	3.86	4.08	-33.94	-74.27	-33.94	-32.11	-33.94
P3	4.47	9.79	4.47	4.23	4.47	-3.26	-7.13	-3.26	-3.08	-3.26	27.10	59.30	27.10	25.64	27.10
P4	3.68	8.06	3.68	3.48	3.68	2.68	5.86	2.68	2.53	2.68	-22.26	-48.71	-22.26	-21.06	-22.26

observed, however, that as the amine content of microgel samples increased, the degree of degradation also increased.

*The model derivations were estimated using reaction mechanisms. For the p (HPMA-Cl), p (HPMA)-TAEA and p(HPMA)-PEI microgels, the most suitable reaction mechanisms for the thermal degradation seem to be the nucleation and nuclei growth models.

*The values of activation energy have been estimated using the Kissinger-Akahira Sunose (KAS), Flynn-Wall-Ozawa (FWO), Coats-Redfern, Ozawa and Friedman methods. The values of activation energy obtained using the kinetic methods showed variations. The results were also in correlation with the kinetic model.

*For p(HPMA-Cl), which had four stages of degradation process, total mass loss achieved was 91.27%. The thermal degradations models were D_1, $F_{1/3\ (n:3)}$, $R_{3\ (sphere/cube)}$, B_1, $A_{3\ (Random\ nucleation\ and\ growth\ of\ nuclei,\ n:3)}$ and P_2.

*For p(HPMA)-TAEA, which had three stages of degradation process, total mass loss achieved was 93.04%, and the thermal degradation models were D_1, $F_{0\ (n:0)}$, $R_{1\ (cylinder)}$ and $A_{4\ (Random\ nucleation\ and\ growth\ of\ nuclei,\ n:4)}$ and P_2.

*For p(HPMA)-PEI, which had four stages of degradation process, the total thermal decomposition was about 75.87%. The means of thermal degradation model were D_1, $F_{0\ (n:0)}$, $R_{2\ (cyclinder)}$, $A_{4\ (Random\ nucleation\ and\ growth\ of\ nuclei,\ n:4)}$ and P_2.

*The stability of microgels were found to have been effected by two factors. These factors are the interactions among amine groups, and the hydrogen-bonds with hydroxyl groups.

*The thermal degradation analysis showed that the activation energy varies with the conversion degree as a consequence of multiphase reactions and the physical changes that the reactions produced in the modified microgels. The activation energy associated with reaction was lower and substantially different than the activation energy obtained at a low degree of conversion associated with main chain breakage.

Reference

1. A. Khawam, D. Flanagan, Solid-state kinetic models: Basics and mathematical fundamentals, J. Phys. Chem. B, 110, (2006), 13.
2. N. Sbirrazzuoli, L. Vincent, A. Mija, N. Guigo, Integral, differential and advanced isoconversional methods. Complex mechanisms and isothermal predicted conversion–time curves, Chemometrics and Intelligent Laboratory Systems, 96, (2009), 7.
3. S. Vyazovkina, A.K. Burnham, J.M. Criado, L.A. Pérez-Maqueda, C. Popescu, N. Sbirrazzuoli, Ictac kinetics committee recommendations for performing kinetic computations on thermal analysis data, Thermochimica Acta, 520, (2011), 19.
4. L.Z. I. Halikia, E. Christodoulou, D. Prattis, Kinetic study of the thermal decomposition of calcium carbonate by isothermal methods of analysis, The European Journal of Mineral Processing and Environmental Protection, 1, (2001), 3.
5. H. Bayrakçeken, J. Naktiyok, H. Okur, A.K. Özer, M. Şahin Gülaboğlu, Non-isothermal calcination kinetics of phosphate rock, Pamukkale Univ J Eng Sci,, 20, (2014), 5.
6. S. Gopalakrishnan, R. Sujatha, Comparative thermoanalytical studies of polyurethanes using coats-redfern, broido and horowitz-metzger methods, Der Chemica Sinica, 2, (2011), 14.
7. C.M. Wyandt, Flanagan, D.R., Solid-state non-isothermal kinetics of sulfonamide-ammonia adduct desolvation., hermochimica acta, 196, (1992), 10.
8. A.K. Burnham, R.K. Weese, B.L. Weeks, A distributed activation energy model of thermodynamically inhibited nucleation and growth reactions and its application to the â-ä phase transition of hmx, J. Phys. Chem. B, 108, (2004), 9.
9. J.T. Carstensen, Stability of solids and solid dosage forms, Journal of Pharmaceutical Sciences,, 63, (1974), 14.
10. L. Liqing, C. Donghua, Application of iso-temperature method of multiple rate to kinetic analysis. , Journal of thermal analysis and calorimetry 78, (2004), 10.
11. J.M. Morancho, J.M. Salla, A. Cadenato, Fernández-Francos, X.,, X. Ramis, P. Colomer, Y. Calventus, R. Ruíz, Kinetic studies of the degradation of poly(vinyl alcohol)-based proton-conducting membranes at low temperatures, Thermochimica Acta, 521, (2011), 8.
12. M.E. Brown, 'Handbook of thermal analysis and calorimetry', Vol. 1, Elsevier, Amsterdam, 1998.
13. M.H. Özyurtkan, D. Özçimen, A.E. Meriçboyu, Investigation of the carbonization behavior of hybrid poplar, Fuel Processing Technology, 89, (2008), 5.
14. C. Gai, Y. Zhang, W.T. Chen, P. Zhang, Y. Dong, Thermogravimetric and kinetic analysis of thermal decomposition characteristics of low-lipid microalgae, Bioresour Technol, 150, (2013), 139-148.
15. Y.C. Hsieh, Y.C. Chou, C.P. Lin, T.F. Hsieh, C.M. Shu, Thermal analysis of multi-walled carbon nanotubes by kissinger's corrected kinetic equation, Aerosol and Air Quality Research, 10, (2010), 6.

16. A.K. Galwey, M.E. Brown, 'Thermal decomposition of ionic solids: Chemical properties and reactivities of ionic crystalline phases.', Vol. 86, Elsevier, Northern Ireland, 1999.
17. S. Ceylan, Kinetic analysis on the non-isothermal degradation of plum stone waste by thermogravimetric analysis and integral master-plots method, Waste Manag Res, 33, (2015), 345-352.
18. A. Khawam, Doctora University of Iowa, Iowa City, 2007.
19. E. Kaya, A. Kurt, M. Er, Thermal degradation behavior of methyl methacrylate derived copolymer, Journal of Nanoscience and Nanotechnology, 12, (2012), 11.
20. V. Mamleev, S. Bourbigot, M. Le Bras, S. Duquesne, J. Sᴄestak, Modelling of nonisothermal kinetics in thermogravimetry, Phys. Chem. Chem. Phys.,, 2, (2000), 8.
21. M. Venkatesh, P. Ravi, S.P. Tewari, Isoconversional kinetic analysis of decomposition of nitroimidazoles: Friedman method vs flynn-wall-ozawa method, J Phys Chem A, 117, (2013), 10162-10169.
22. R. Ebrahimi-Kahrizsangi, Abbasi, M.H., Evaluation of reliability of coats-redfern method for kinetic analysis of non-isothermal tga, Transactions of Nonferrous Metals Society of China 18, (2008), 4.
23. A. Aboulkas, K. El harfi, A. El bouadili, M. Nadifiyine, M. Benchanaa, A. Mokhlisse, Pyrolysis kinetics of olive residue/plastic mixtures by non-isothermal thermogravimetry, Fuel Processing Technology, 90, (2009), 6.
24. Ç. Kip, B. Maraş, O. Evirgen, A. Tuncel, A new type of monodisperse porous, hydrophilic micro spheres with reactive chloroalkyl functionality: Synthesis and derivatization properties. , Colloid Polym Sci, 292, (2014), 9.
25. N. Sahiner, A. Attaa, A. Yasar, H. Al-Lohedan, A. Ezzat, Surface activity of amphiphilic cationic ph-responsive poly(4-vinylpyridine) microgel at air/water interface, Colloids and Surfaces A: Physicochemical and Engineering Aspects, 482, (2015), 8.
26. B. Çelebi, A. Gökaltun, E. Arman, O.A. Evirgen, A. Tuncel, Polyethylenimine attached-poly(3-chloro-2-hydroxypropyl methacrylate-co-ethylene dimethacrylate) monosized-porous microspheres as a new separation medium for polar compounds, Colloids and Surfaces A: Physicochemical and Engineering Aspects, 441, (2014), 8.
27. N. Sahiner, A.O. Yasar, The generation of desired functional groups on poly (4-vinyl pyridine) particles by post-modification technique for antimicrobial and environmental applications, Journal of colloid and interface science, 402, (2013), 6.
28. A. Khawam, D. Flanagan, Basics and applications of solid-state kinetics: A pharmaceutical perspective, Journal of Pharmaceutical Sciences, 95, (2006), 27.
29. A. Aboulkas, K. El Harfı, Study of the kınetıcs and mechanısms of thermal decomposıtıon of moroccan tarfaya oil shale and its kerogen, Oil Shale, 25, (2008), 7.
30. A. Aboulkas, K. El harfi, A. El Bouadili, Thermal degradation behaviors of polyethylene and polypropylene. Part i: Pyrolysis kinetics and mechanisms, Energy Conversion and Management, 51, (2010), 6.
31. J.J.M. Orfao, F.G. Martins, Kinetic analysis of thermogravimetric data obtained under linear temperature programming—a method based on calculations of the temperature integral by interpolation, Thermochimica Acta, 390, (2002), 6.
32. R.L. Blaine, B.K. Hahn, Obtaining kinetic parameters by modulated thermogravimetry, Journal of Thermal Analysis, 54, (1998), 9.
33. M.B. Folgueras, R.M. Dı´az, J. Xiberta, I. Prieto, Thermogravimetric analysis of the co-combustion of coal and sewage sludge, Fuel, 82, (2003), 4.
34. Ramos-Fernandez, E.V., N.R. Shiju, G. Rothenberg, Understanding the solar-driven reduction of co2 on doped ceria, RSC Advances, 4, (2014), 7.
35. A. Khawam, D. Flanagan, Complementary use of model-free and modelistic methods in the analysis of solid-state kinetics, J. Phys. Chem. B, 109, (2005), 7.
36. G. Bayramoglu, M.Y. Arica, Polyethylenimine and tris(2-aminoethyl)amine modified p(ga-egma) microbeads for sorption of uranium ions: Equilibrium, kinetic and thermodynamic studies, J Radioanal Nucl Chem, 312, (2017), 10.